國立臺灣大學理學院心理學研究所

碩士論文

Graduate Institute of Psychology

College of Science

National Taiwan University

Master Thesis

空間位置的調節與物體特徵的整合於工作記憶的

神經機制探討：腦磁圖研究

Neural Correlates for Location-Shared and Feature-Bound

Representations in Visual Working Memory:

An MEG Study

陳雅苹

Ya-Ping Chen

指導教授：郭柏呈博士

Advisor: Bo-Cheng Kuo, Ph.D.

中華民國 107 年 7 月

July, 2018

誌 謝

這趟碩士論文之旅既華麗且瘋狂，它的豐富來自於以各種形式參與的每一個人。希望有限的文字能夠乘載我無邊的感謝。

最要感謝指導教授郭柏呈老師的教導、勉勵、關懷與信任，使這篇論文得以擺脫貧乏無趣、邏輯缺陷與證據不足，也讓與這篇論文同時成長的我，在這短暫的不到兩年的時間完成許多心中的小夢想：普心助教、心實助教、德文助教、德國生活，沒有老師的支持，就沒有這不可思議燦爛的六百多個日子。感謝研究計畫的共同主持人 Jun Saiki 教授，Saiki 老師多次從日本飛來臺灣給予指教並擔任口試委員，讓我有機會潛入行為模型的領域一探究竟，每一次與 Saiki 老師的討論都是收穫滿載。感謝口試委員葉怡玉教授和阮啟弘教授，老師們百忙之中費心閱讀論文，帶領我從基本的理論檢視實驗設計並且提醒注意參數設定背後的假設與限制，老師們的建議也讓我有機會從不同的觀點詮釋這篇論文以及未來可以努力的方向。

謝謝實驗室夥伴們專業上的無私分享與生活裡的陪伴照顧。謝謝律君在口試期間的全力協助，讓我在繁雜的口試前置準備過程中可以全然安心地只負責報告與答辯內容，可以在最後一秒才踏入口試現場，以及平時眾多分析結果和統計上的顧問。謝謝雅婷分享伽瑪波的文獻與協助張羅口試委員們的餐點，還有平日對實驗室大小事的精確掌握和熱心幫助，讓我多次坐享其成。謝謝俊輝在口試時的技術資源，以及平時機器學習專業知識的分享，讓我可以與世界潮流接軌。謝謝芳雯在方法章節的協助，讓我在撰寫論文的最一開始能有個平穩的起飛，也謝謝在心實助教、德文助教、德國生活，每個小夢想中的強力支援，你的點滴陪伴使他們近乎完美。

謝謝長久以來從不間斷給予愛護的師長與朋友們。謝謝蔡嘉穎老師讓我在口試最後的準備期間可以暫時拋棄學生們專注準備，以及一次次加油打氣和灌注信心。謝謝室友祐蓁，容忍我在口試前讓深夜裡的房間滿是光害的日子。謝謝悠綸不時的小關心，積沙成塔地成了堅實的堡壘。謝謝麗玲溫暖的擁抱，成為我堅定前進的動力。

最後感謝我優秀的父母、妹妹、弟弟，讓我擁有選擇的自由，給予經濟支持，甚至良好的生活品質，可以心無旁騖地完成碩士學業。

摘要

　　過去研究指出具有多重特徵的物體會以整合的形式表徵於工作記憶中。雖然這些研究結果顯示空間位置在視覺工作記憶中的特徵整合扮演重要的角色，然而物體的空間位置與工作記憶中特徵整合表徵的神經機制仍有待進一步的研究。在本研究中，我藉由視覺工作記憶作業典範，並結合修正的「冗餘增益」派典、行為模型和腦磁圖，探討空間位置對物體於工作記憶表徵特徵整合調節的神經機制。共有十八位健康成人參與腦磁圖實驗，在進行實驗的記憶過程中，實驗參與者首先會同時看到並要記住兩個物體，這兩個物體皆具有兩個特徵—字母和顏色，經過短暫的記憶維持階段後，實驗參與者必須在測驗階段中指出此時出現的物體是否具備記憶物體的任一特徵(字母或顏色)，此一判斷不須考慮物體的空間位置。我首先使用「賽跑模式不等式」檢驗受試者的反應時間，反應時間的累積密度函數顯示，當測驗階段呈現的物體同時具有記憶物體的兩個特徵時，會出現特徵共活化的現象並支持特徵連結的假設，而此現象不受到特徵空間位置的影響。無論特徵位置改變與否，當物體以特徵整合的形式呈現時，我在頂葉皆可以觀察到較強烈的 Gamma 波。最後，我以時間序列的結果支持特徵整合發生在後頂葉與視覺皮質。這些研究結果支持了物體的特徵整合不會受到空間位置改變的影響。

關鍵詞：工作記憶、特徵連結、物體位置、冗餘增益、Gamma 波

Neural Correlates for Location-Shared and Feature-Bound Representations in Visual Working Memory: An MEG Study

Ya-Ping Chen
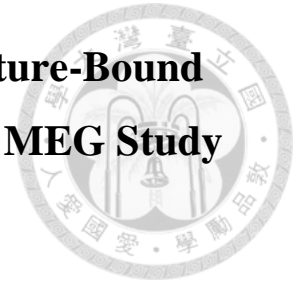
Abstract

Previous studies have shown that feature-integrated object representations are formed in visual working memory (WM). While these findings highlighted the importance of spatial location in feature binding in visual WM, the underlying neural substrates of location-shared and feature-bound representations in visual WM were not fully investigated. Here I address this issue in a visual WM task with a modified redundancy-gain paradigm, using behavioral modeling and magnetoencephalograhy (MEG). In this study, participants (N = 18) performed a WM task in which they viewed two types of feature (colors and letters) in a two-object memory display, following a short delay, and a single object probe. Their task was to indicate whether the probe item contained any feature in the memory display, regardless of its location. I firstly conducted a *race model inequality* (*RMI*) test to examine the response time (RT) data. The cumulative density function of the RT suggested feature integration when the probe item contained two features regardless of its location. Next, I found significant gamma activity in the parietal cortex for feature-bound representations in both shared- and unshared-location conditions. Finally, the time-series data confirmed the feature-bound effect in posterior parietal and early visual areas. In conclusion, the results provide novel evidence in behavioral and neural measures and suggest that feature-bound representations can be independent to object location.
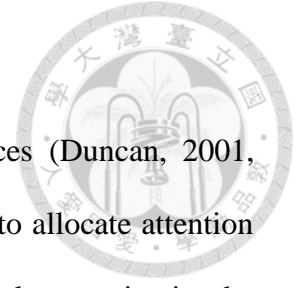
Keywords: *working memory, feature binding, object location, redundancy gain, gamma-band activity*

Contents

Introduction

Humans exhibit remarkable flexibility to adapt to novel circumstances (Duncan, 2001, 2013). This cognitive flexibility in humans relies heavily on our brain to allocate attention toward the information that is relevant to the immediate goals and to maintain the information in working memory (WM) over time. Despite the unquestioned progress of research on attention and WM to date (Awh, Vogel, & Oh, 2006; Chun & Johnson, 2011; Gazzaley & Nobre, 2012; Jonides et al., 2008; Myers, Stokes, & Nobre, 2017), the underlying mechanisms for the comparisons of perceptual inputs with the contents of WM remain largely uninvestigated. In this study, I test whether the to-be-remembered feature-bound and feature-unbound representations can be influenced by their spatial locations during the WM-perceptual comparisons using behavioral modeling and magnetoencephalography (MEG).

WM is the cognitive construct to bridge the gap between perception and higher-level mental processes such as long-term memory (LTM), thinking, reasoning, and language (Baddeley, 1986, 1992; Cowan, 1999). However, the capacity of visual WM is limited (Cowan, 2001; Luck & Vogel, 1997) – only three or four units of information can be maintained at a given instance. Extensive evidence has revealed that the WM capacity limit can be determined by the number of individual items (Edin et al., 2009; Zhang & Luck, 2008) and varied across individuals (Luck & Vogel, 2013). These studies showed that WM is constrained to represent a set of discrete units or objects. The integrated objects, instead of distinct features, are retained to form the WM contents. For example, evidence from electrophysiological recordings in humans revealed that the maintenance-related

1

event-related potential (ERP), known as "contralateral delay activity" (CDA) or "sustained posterior contralateral negativity" (SPCN) shows a sustained activity throughout the delayed period and scales with the number of maintained items in WM (Fukuda & Vogel, 2009). The amplitude of CDA reached a limit when the maintained items were approximately four, suggesting no increase from four to six or eight items (Vogel & Machizawa, 2004; Vogel, McCollough, & Machizawa, 2005). Moreover, the CDA amplitude can only be accounted for integrated objects regardless of the number of features or visual complexity (Luria & Vogel, 2011). These findings suggest that visual WM can maintain up to three or four bound objects instead of separate features.
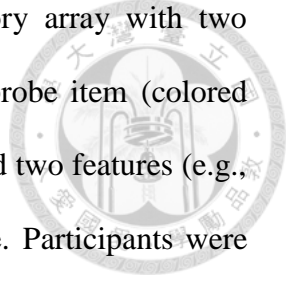
Accumulating behavioral and neural studies have also focused on the topic of feature binding or feature integration in visual WM (Allen, Baddeley, & Hitch, 2006; Fitousi, 2018; Klimesch, Freunberger, & Sauseng, 2010; Sala & Courtney, 2007; Schneegans & Bays, 2017; Shafritz, Gore, & Marois, 2002; Treisman & Zhang, 2006; Wheeler & Treisman, 2002). In particular, these studies highlighted the importance in the association of the objects with their spatial locations (Hollingworth & Rasmussen, 2010; Treisman & Zhang, 2006; Van Dam & Hommel, 2010; Wang, Cao, Theeuwes, & Olivers, 2016). These short-lived and feature-bound representations, i.e. object files (Kahneman, Treisman, & Gibbs, 1992), contained the combination of different features and their perceptual continuity as an object. According to the object file account, the spatial location may serve as the nexus to bind features into an object. For example, the WM performance in a change detection task can be impaired when task-irrelevant object location was changed in a test array, relative to a memory array (Hollingworth & Rasmussen, 2010; Kondo & Saiki, 2012; Saiki & Miyatsuji, 2007; Yang, Fan, Wang, Fogelson, & Li, 2017). These results suggest

2

that location may influence object representations and attention can be guided to the locations of the objects that match the to-be-remembered contents in visual WM.
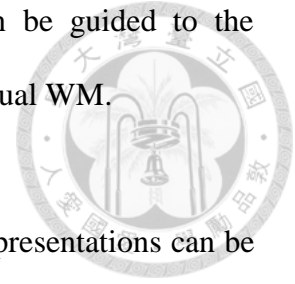
Although previous studies have shown that the feature-bound object representations can be mediated by their spatiotemporal coordinates (Hollingworth & Rasmussen, 2010; Treisman & Zhang, 2006; Van Dam & Hommel, 2010), other studies, however, suggest a privileged role of bound representations in visual WM relative to their locations (Logie, Brockmole, & Jaswal, 2011; Saiki, 2016). For example, Logie et al. (2011) examined the extent to which location, color and shape may contribute to feature binding in visual WM at varying retention intervals. Their results were contrary to the predictions from the object file account. They showed that the feature-bound representation in visual WM was not affected by task-irrelevant changes of location as well as shape and color. Moreover, similar findings were reported by a recent study (Saiki, 2016). In his study, the amount of feature (two features, one feature, and no feature) and location sharing between memory and probe items were both manipulated during the WM and perceptual comparisons. His results demonstrated that the advantage of feature binding occurs only in the feature-bound condition compared to one-feature condition regardless of location sharing. Together, these studies suggest that feature binding in WM may not be necessarily dependent upon location.

The goal of this study was to investigate the cognitive and neural mechanisms of the role of spatial location on feature-bound representations during the comparisons of WM and perception. I test whether the to-be-remembered feature-bound and feature-unbound representations can be influenced by their locations in a WM task with a modified

3

redundancy-gain paradigm. In the task, participants viewed a memory array with two colored letters, following a short delay, and a probe array with one probe item (colored letter) and one non-target percentage sign (%). The probe item contained two features (e.g., letter and color), one feature (e.g., letter or color), or no target feature. Participants were instructed to remember all object features regardless of their locations and indicate whether the probe item contains at least one feature from the memory array. I firstly compared the response times (RTs) for the one-feature trials to the RTs for the two-feature trials using the race-model-inequality (RMI) test (Miller, 1982; Saiki, 2016). I evaluated whether the redundancy gain from the bound features can surpass the limit of independent processing of two distinct features. If feature binding occurred for the bound representations, faster RTs should be expected for the feature-bound condition compared to the one-feature condition. That is, the RMI would be violated because two distinct features are bound as an integrated or grouped object (Feintuch & Cohen, 2002; Mordkoff & Danek, 2011).

Importantly, I explore the oscillatory correlates of WM-perceptual comparisons for feature-bound and feature-unbound representations. Previous studies have shown that gamma-band oscillations (30-80 Hz) are involved in the maintenance of relevant information in WM (Honkanen, Rouhinen, Wang, Palva, & Palva, 2015; Roux & Uhlhaas, 2014; Roux, Wibral, Mohr, Singer, & Uhlhaas, 2012) and could be critical marker of local, cortical interactions involving neural excitation and inhibition (Fries, 2015; Fries, Reynolds, Rorie, & Desimone, 2001; Ray & Maunsell, 2015). Recent studies also showed that gamma activity in the parietal cortex was higher for the operation of feature binding than the single feature in WM (Morgan et al., 2011). Using anti-phase gamma stimulation over the left

4

temporal and parietal cortex, an enhanced effect was found for color-shape bound trials (Tseng, Chang, Chang, Liang, & Juan, 2016).
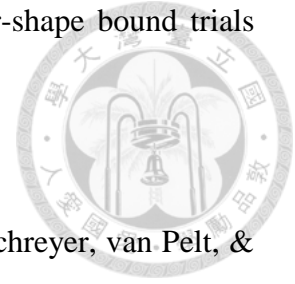
Here I tested whether the target-related gamma oscillations (Landau, Schreyer, van Pelt, & Fries, 2015; Poch, Campo, & Barnes, 2014) could be modulation by location sharing during the comparisons. I also explored the neural originals of the gamma oscillations for both feature-bound and feature-unbound representations respectively. If feature binding cannot be influenced by their spatial locations, I predicted significant gamma activity for comparing bound representations with their WM contents irrespective of spatial locations.

Finally, the event-related time-series data (event-related field, ERF) was also analyzed. I sought to test the load-dependent effect of WM (Kuo, Rao, Lepsien, & Nobre, 2009; Nobre, Griffin, & Rao, 2008). If feature binding occurs when two distinct features belong to a single object, I would predict an increase in ERF for two features which were not bound to a single object. If object representations were not necessarily bound to their locations, I would also expect no differences in ERF between the trials with shared locations versus the trials with unshared locations for the bound representations. I also test for the neural sources of the load-dependent effect.

Methods
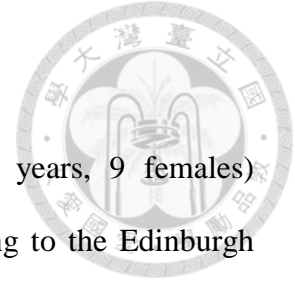
Participants

Twenty healthy volunteers (mean age = 24 years, range = 20-29 years, 9 females) participated in this study. All participants were right-handed, according to the Edinburgh handedness inventory (Oldfield, 1971), with normal color vision and normal or corrected-to-normal visual acuity. They were provided with both verbal and written informed consent prior to the study and were financially reimbursed for their time. Data from two male participants were excluded from analysis due to excessive artifacts in the MEG data (more than 30% trials) or slow response time (over three standard deviations). All experimental materials and procedures were reviewed and approved by Research Ethics Committee of National Taiwan University.

Stimuli

The setting of stimuli size and colors in this study were identical to those in Saiki's study (2016). Memory and probe arrays were composed of colored letter stimuli. Four capital letters (K, M, P, S) and four colors (red, blue, green, yellow) were selected. Each letter was $1.68°$ visual angle in size and positioned in one of the two visual hemifields at a visual angle of approximately $4°$ away from a central fixation point. The combination of letters and colors was fully counterbalanced so that all the letter-color pairs were presented with equal frequency. All of the visual stimuli were presented against a homogeneous grey background. The stimuli were generated and delivered in Matlab (The MathWorks, Natick, MA), using the Psychophysics Toolbox extensions (Brainard, 1997).

Task Design

Main WM task. The task procedure is illustrated in Figure 1. Each trial began with a centrally displayed fixation for 750 ms, which signaled the onset of the trial. Next, a display consisting two unfilled square boxes (2.1° x 2.1° in size), one in each hemifield at a visual angle of approximately 4° away from the central fixation point, was present for 750 ms. After that, a memory array consisting of two colored letters, one inside each box, was present for 250 ms. Participants were instructed to remember both letters and colors within the memory array. Following a randomized retention interval (with boxes alone, 1250 - 1750 ms duration), a single probe letter in color was shown in one of the boxes with a percentage sign (%) in another square for 500 ms. Participants were instructed to decide whether the feature (letter or color) of the probe item had been present in the memory array, regardless of the location of the to-be-remembered items, by pressing left or right button using their left or right index finger. The assignment of left and right buttons for target present and absent was counterbalanced across participants.

I manipulated the number of features for the probe item. The probe item contained two features (grouped and separated conditions), one feature (letter-match and color-match conditions), and no features relative to the features in the memory array. In the two-feature condition, the probe contained the identical combination of the letter and the color from one of the memory items (grouped condition) or the color from one item and the letter from the other (separated condition). In the one-feature condition, the probe contained only a single feature from one of the memory items (letter-match condition and color-match condition). In the no-feature condition, the probe did not contain any colors or letters from the memory items.
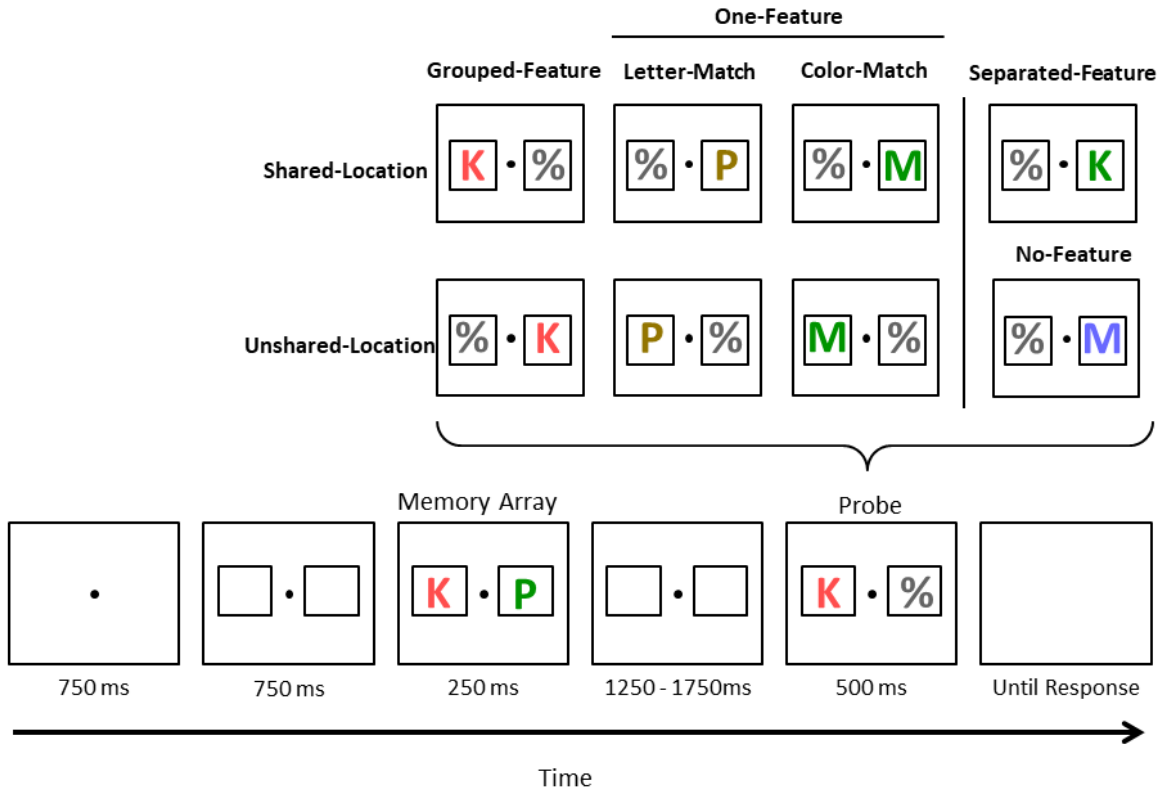
7

Figure 1. Schematic of the main WM task. There were eight types of probes relative to the stimuli in the memory array. Participants were instructed to remember two two-feature (letter and color) objects regardless of their locations and to indicate whether any feature in the probe array was presented in the memory array.

More importantly, I manipulated location-sharing for the grouped and one-feature conditions. That is, the features of probe items matched the memory items in the same box (e.g. in the visual hemifield) for shared-location trials; by contrast, the features of the probe items matched the memory items in the different box (e.g. in the opposite visual hemifield) for unshared-location trials. In sum, there were eight types of probes: grouped-shared, grouped-unshared, letter-shared, letter-unshared, color-shared, color-unshared, separated, and no feature. The two-feature conditions contained grouped-shared, grouped-unshared, and separated trials. The one-feature conditions contained letter-shared, letter-unshared, color-shared, and color-unshared trials. The shared condition contained grouped-shared, letter-shared, and color-shared trials. The unshared condition contained grouped-unshared, letter-unshared, and color-unshared trials. In all conditions, half of the trials of the probe items were shown in the right hemifield and the other half were shown in the left hemifield.

Visual localizer task. To identify the region of interest (ROI) in early visual areas that respond selectively to the locations of the visual stimuli, participants also performed a visual localizer task (Figure 2). Participants were instructed to view the stimuli passively without making any responses. Gabor patches, with one of four colors (the same colors used in the main task), were presented in the same size and at the same location as in the main task and were tagged at different frequencies (1.38 and 1.76 Hz) (see Baldauf & Desimone, 2014 for an example). There were four conditions in the localizer task: 2 (frequency: 1.38 and 1.76 Hz) x 2 (hemifield: left and right). In each condition, there were eight blocks with the Gabor patch presented 20 times. The order of the blocks was counterbalanced across participants. The stimuli were presented with Presentation software (Neurobehavioral Systems, Albany, NY, USA).
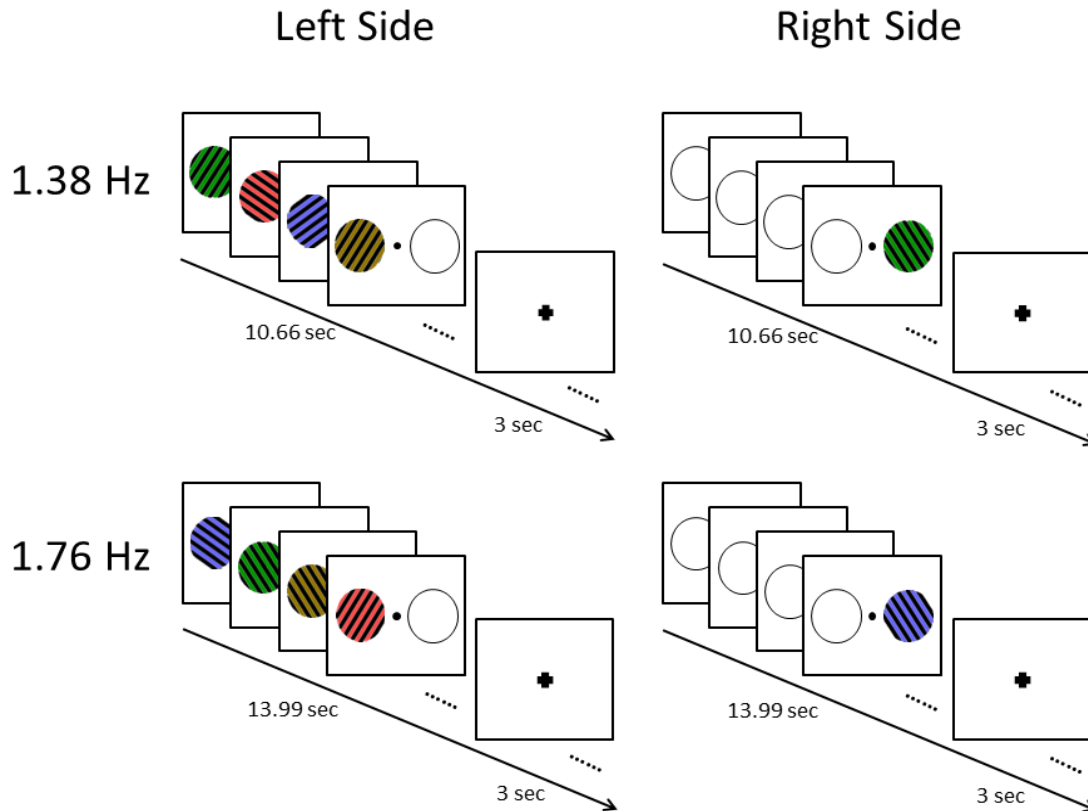
Figure 2. Examples of the visual localizer task. Gabor patches were showed in one of the four colors used in the WM task and in the same size as the objects in the WM task. There were four conditions: two frequencies (1.38 Hz and 1.76 Hz) and two hemifields (right and left). Participants were instructed to view passively through all four conditions.

Experimental Procedure

Participants were comfortably seated in a magnetically and electrically shielded room, 120 cm from the screen on which the stimuli were projected. All participants were given written and verbal instructions for the tasks. They were also instructed to minimize their head movements, eye movements and blinks during the tasks and maintain fixation on a small marker at the center of the screen throughout the experiment and to respond as accurately and quickly as possible. Prior to the actual experiment, each participant completed one practice block of 48 trials. For the main WM task, participants completed five runs (including 3 blocks for each run and 48 trials for each block, 720 trials in total), with the rest periods being self-paced between blocks in each run. Of all the 720 trials, there were 240 two-feature trials (120 grouped trials and 120 separated trials), 240 one-feature trials (120 letter-match trials and 120 color-match trials), and 240 no-feature trials. Half of grouped and half of one-feature trials were location shared. All of the trial types were intermixed in a randomised and unpredictable order. Participants completed the visual localizer task right after the main WM task. MEG recording time for each participant was approximately 100 minutes. A video camera installed inside the MEG chamber allowed monitoring of the participants' behavior and compliance throughout the experiment.

Behavioral Analysis

Two types of analysis were performed on behavioral data. First, I tested the difference in three two-feature conditions (grouped-shared, grouped-unshared, separated) with one-way repeated-measures analysis of variance (ANOVA) and the modulatory effect of shared location for the grouped-match, color-matched, and letter-match conditions in a 3 (feature

11

type: grouped, letter-feature, color-feature) x 2 (location type: shared, unshared) repeated-measures ANOVA. The behavioural measures, including accuracy and reaction times (RTs), were each analysed and only correct responses were included in the RT analyses.
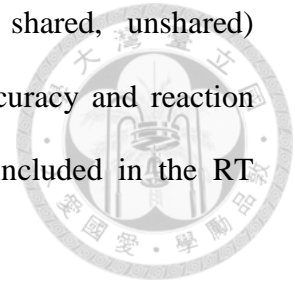
Second, I conducted the RMI test (Miller, 1982; Mordkoff & Yantis, 1991) on RT data to evaluate whether the redundancy gain could be accounted by the separate-activation models (Raab, 1962) using the following inequality (see also Saiki, 2016):

$$p\,(RT < t \mid F_1 \text{ and } F_2) \ \leq \ p\,(RT < t \mid F_1) + p\,(RT < t \mid F_2)$$

where t equals time, and F_1 and F_2 stand for the two types of features respectively.

In this analysis, trials with incorrect responses or the trials with long RT (> 3000 ms) or short RT (< 150 ms) were excluded. The inequality states that the cumulative probability of any given RTs for the two-feature trials (grouped, separated) never exceeds the sum of the cumulative probability of the RTs for the letter-match and color-match trials alone. According to the separate-activation models, the upper boundary of RTs in the two-feature conditions can be defined by the RMI. Thus, violation of the RMI indicates feature coactivation (e.g. faster RTs in the two-feature condition than the upper boundary of RTs). The feature coactivation effect can be used as an index of feature binding (Saiki, 2016). The violation of the RMI was evaluated in the following steps (Mordkoff & Danek, 2011; Saiki, 2016): (1) for each subject, the values of RT corresponding to the 5th through 95th percentile (at 5% intervals) were computed for the two-feature trials and the sum of the percentiles of one-feature trials (letter-match and color-match); (2) The overall 19-point

12

cumulative density functions (CDF) were formed by simply averaging all the RTs at each percentile across subjects; (3) At each percentile, a one-tailed paired *t* test was performed to examine the difference in mean RT values between the two-feature condition and the sum of the one-feature conditions with the null hypothesis that the difference is zero or a negative value.
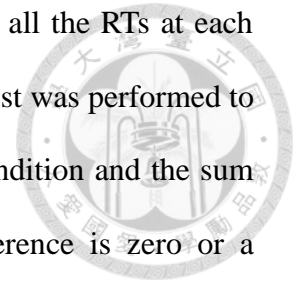
MEG Acquisition and Recording Parameters

MEG data were recorded using a 306-channel Triux system (Elekta Neuromag), with 102 magnetometers and 204 orthogonal planar gradiometers (pairs of sensors measuring the longitudinal and latitudinal derivatives of the magnetic field) at the Imaging Center for Integrated Body, Mind, and Culture Research, National Taiwan University, Taipei, Taiwan. The signals had a sampling rate at 1000 Hz, and were band-pass filtered between 0.03-330 Hz. Head position was monitored by four head position indicator (HPI) coils placed on the scalp, indicating the position of the head in the MEG helmet during recording. A digitizer (Polhemus, USA) was also be applied to digitize three fiducial landmarks (the nasion, left and right pre-auricular points), four HPI coils, and a number of additional head points for further alignment with individual T1-weighted structural MRI images. Vertical eye movements were recorded by MEG-compatible electrodes placed on the supraorbital ridges of the left eye [vertical electro-oculogram (VEOG)], and the horizontal eye movements by electrodes placed on the outer canthi of the right and left eyes [horizontal electro-oculogram (HEOG)]. Both VEOG and HEOG were recorded and subsequently used to remove trials contaminated by blinks or eye movements.

Structural MRI Acquisition and Scanning Parameters for MEG Analysis

High resolution anatomical images (1 x 1 x 1 mm) were acquired from all participants by a T1-weighted MPRAGE sequence (FOV = 192 x 192 mm) on a Siemens 3T MAGNETON Prisma MRI scanner with a 20-channel coil at the Image Center for Integrated Body, Mind, and Culture Research, National Taiwan University, Taipei, Taiwan.

MEG Data Analysis

External noise was firstly removed from the MEG data using the signal space separation (SSS) method implemented in Elekta's MaxFilter software. All MEG data processing and analysis were then carried out using SPM8 software (Wellcome Trust Centre for Neuroimaging, University College London, UK), FieldTrip toolbox (Oostenveld, Fries, Maris, & Schoffelen, 2011) and the in-house scripts in Matlab (The MathWorks). The data from the main WM task and the visual localizer task were processed separately. Four types of analysis were performed on the MEG data. First, I conducted a time-frequency analysis at the sensor level to explore the oscillatory correlates of feature integration. Second, a MEG source-level analysis was used to identify the neural origins in the gamma-band range of feature integration. Third, I examined the event-related field (ERF) data at the sensor level. Finally, I conducted a region-of-interest (ROI) analysis based on the visual localizers and tested for the neural origins of the ERF during feature binding.

Preprocessing. The continuous MEG signals were down-sampled to 250 Hz and low-pass filtered below 120 Hz. For the WM task, the continuous data were segmented into epochs from -1,000 ms to 1,500 ms relative to the onset of the probe and baseline-corrected with
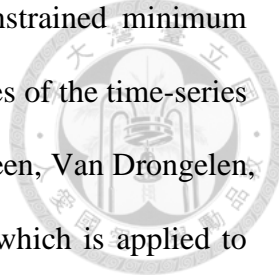
14

the 200 ms pre-probe period. Only correct trials were retained for subsequent analyses. All the epochs were visually inspected for artifact rejection. Through visually detecting VEOG and HEOG for eye-movement artifacts (blinks or saccades), epochs with contamination and excess noise were excluded from subsequent analyses. Trials with unusually high variance were also removed using FieldTrip visual artifact rejection tool.

Sensor-level time-frequency analysis. The artifact-free sensor-space epoched data were entered into time-frequency decomposition, using Morlet wavelets with a length of 7 cycles. The resulting power spectra of the gamma frequency were averaged according to feature types (grouped-shared, grouped-unshared, separated, one-feature-shared, one-feature-unshared) and probe locations within the array (left and right). The time-frequency data containing perceptual targets located on the right and left side in each condition were then combined by an averaging procedure that preserved the location of MEG sensors relative to the target side (contralateral and ipsilateral). That is, for all the feature types I tested for the presence of spatially target-specific modulations at gamma frequency bands (i.e. lateralized gamma power), at the moment when participants compared the visual display of the probe items with their WM contents. For this sensor-space time-frequency analysis, I only used the planar gradiometers. I combined the pairs of planar gradiometers using the Cartesian sum for each participant, producing a 102-channel combined planar gradiometer data set. Power differences for the lateralized gamma activity were tested for every time point between conditions using dependent sample t tests. I then corrected for multiple comparisons using a cluster-based non-parametric permutation approach (Maris & Oostenveld, 2007). We calculated the size of any significant clusters with consecutive t tests that were significant ($p < .05$, two-tails) either across neighbouring

15

sensors, time-points, or both. I calculated Monte Carlo p values on 1,000 random partitions in which left and right probe location were shuffled, thereby deriving a null distribution of the clustered test statistics that would be achieved by chance. Type I errors were thus reduced by controlling multiple comparisons across both sensor and time. Finally, the values ($p < .05$, two-tails) in this null distribution that was greater than the clustered statistics from the original data was treated as the corrected significant value.

Sensor-level ERF analysis. The artifact-free sensor-space ERF epochs were baseline-corrected with the 100 ms pre-stimulus period. Epochs were averaged per condition for each participant. This procedure resulted in five conditions: grouped-shared, grouped-unshared, one-feature-shared, one-feature-unshared, and separated condition. The pairs of planar gradiometers were then combined using the root-mean-square values at each sensor for each participant, producing a 102-channel combined planar gradiometer data set. To test the feature-bound effect in the posterior region, the mean ERF would be extracted from the chosen sensors and two time windows. A 2 (time window: 250-400 ms, 400-550 ms) x 3 (two-feature conditions: grouped-shared, grouped-unshared, and separated) repeated-measures ANOVA was conducted to explore the differential effect among two-feature conditions.

Source analysis for ERF and time-frequency data. I conducted a beamformer analysis to characterize the neural sources of ERF and time-frequency power data from both the magnetometers and planar gradiometers. I firstly co-registered each individual's MEG data based on their T1-weighted structural image using digitized scalp locations and fiducials. A semi-realistic single shell head model (Nolte, 2003) based on each individual's brain was

16

constructed. For testing the neural origins of ERF data, a linear constrained minimum variance (LCMV) beamformer algorithm was used to identify the sources of the time-series effects at every vertex of a 7-mm grid covering the whole brain (Van Veen, Van Drongelen, Yuchtman, & Suzuki, 1997). Beamforming constructs a spatial filter, which is applied to the sensor data to reconstruct the signal at each grid point, with the aim of achieving unit bandpass response at the grid point while minimizing the variance passed from all other locations. The data at the source location of interest are given by multiplying the beamformer weights vector by the original sensor data. The process can be repeated across all grid locations to achieve a whole brain source reconstruction for each time point. The source analyses were performed for each condition. The source estimates of the individual subjects' functional data were interpolated to their own structure image and then spatially normalized to the MNI brain. Finally, the statistical differences in source activity between conditions were computed using the non-parametric permutation approach (Maris & Oostenveld, 2007). The source analysis of the oscillatory activity was estimated by the Dynamic Imaging of Coherent Sources (DICS) beamformer algorithm (Gross et al., 2001). The time-frequency parameters were identical to the sensory-space analysis (Morlet wavelet with a length of 7 cycles). The source-analysis parameters were identical to the ERF source analysis.

Power and source analyses for the visual localizer task. Finally, I conducted power and source analyses for the visual localizer task. The MEG preprocessing were identical to those for the main task. I only describe the exceptions below. The visual localizer data were segmented into -1,000 ms to 10,664 ms for the 1.76 Hz condition and 13,996 ms for the 1.38 Hz condition. I first conducted the frequency analysis to confirm the effect of

frequency tagging (Figure 3). The pipeline of the analysis of the visual localizer shows in Figure 4. The DICS technique was then applied for the source analysis. The resulting spatial filters were applied to the Fourier-transformed power based on the frequency of interest (1.76 Hz and 1.38 Hz, respectively). To reduce biases toward the center or the head, I computed the neural activity index (NAI) by dividing the estimated power at each grid point by an estimate of the noise (Mitra & Pesaran, 1999). This noise bias was estimated for each participant's data. After that, the results of the NAI were coregistered on the subject's structural MRI and spatially normalized to the MNI brain. I averaged the NAI results across participants to generate averaged NAI maps. To generate contralateral localizer maps, two contrasts were computed: left target with 1.38 Hz versus right target with 1.76 Hz and right target with 1.38 Hz versus left target with 1.76 Hz. Finally, I combined the contralateral localizer maps with visual maps based on the probabilistic estimates of visual areas from a previous study (Minini, Parker, & Bridge, 2010). This analysis resulted in two visual ROIs (left and right hemispheres).
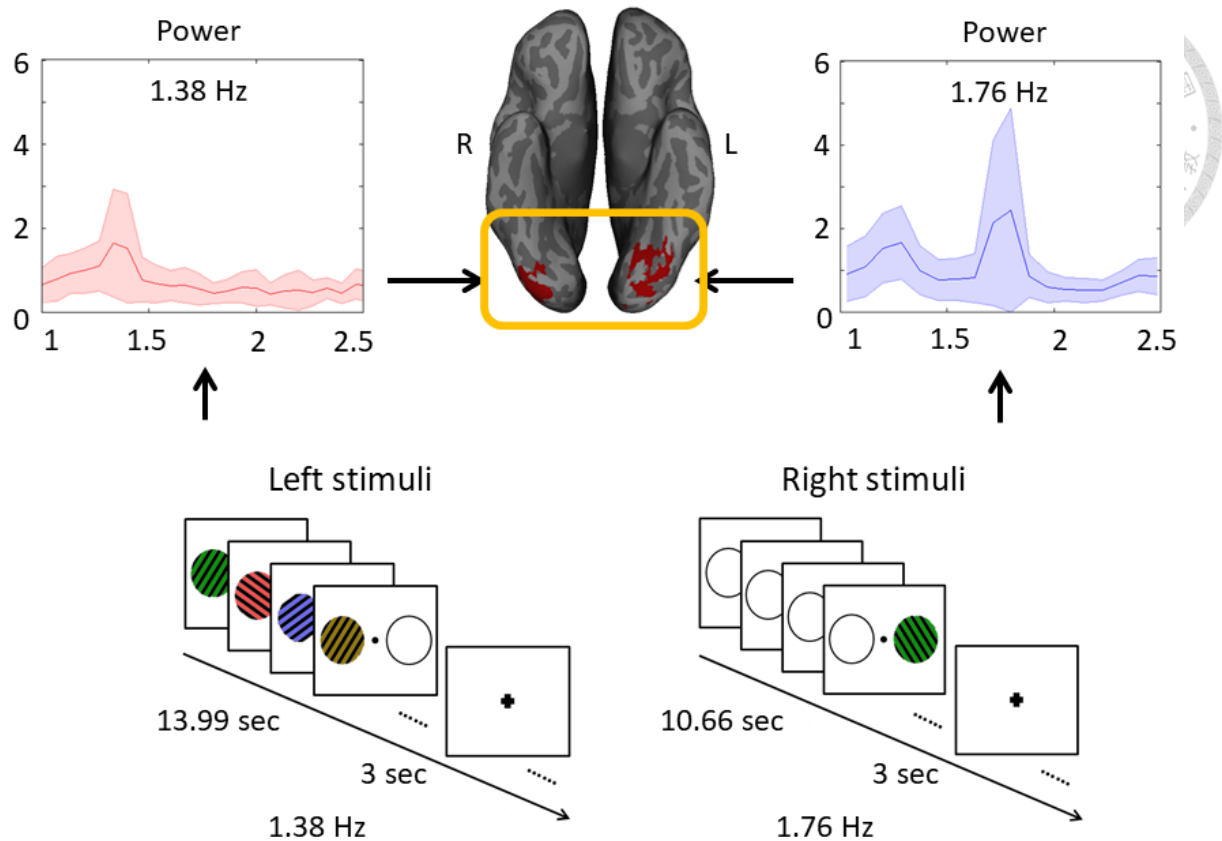
18

Figure 3. Illustration of spectral power in the visual localizer task in left 1.38 Hz and right 1.76 Hz conditions respectively. The results of frequency analysis confirmed the effect of the manipulation of the frequencies (1.38 Hz and 1.76 Hz) and the hemifields (left and right).
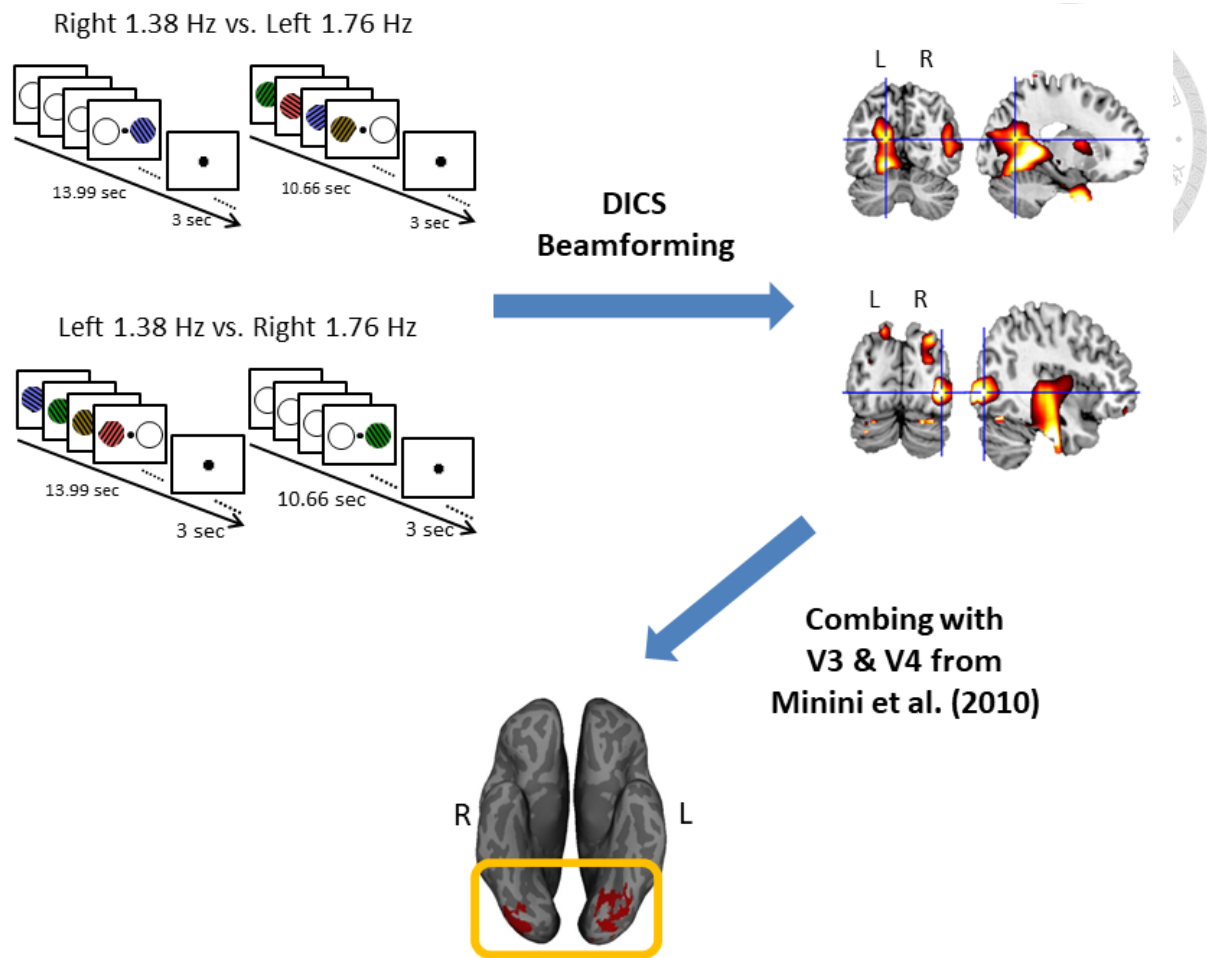
Figure 4. Schematic of the analysis procedure for regions of interest in visual areas: the DICS beamformer was applied to the Fourier-transformed power based on the frequency of interest. To generate contralateal localizer maps for each hemisphere, two contrasts were computed: left target with 1.38 Hz versus right target with 1.76 Hz and right target with 1.38 Hz versus left target with 1.76 Hz. The resulting localizer maps were combined with visual maps from Minini et al. (2010)'s study.

Results

Behavioral Results

Table 1 shows the mean accuracy and mean RTs for the eight conditions. The accuracy data indicated no difference between grouped-shared, grouped-unshared, and separated trials (ps > .1). A 2 (location: shared, unshared) x 3 (feature type: grouped-feature, letter-match, color-match) repeated-measures ANOVA showed a significant main effect of feature type, F (2, 34) = 37.58, p < .001, η_p^2 = .69, and a significant interaction between feature type and location, F (2, 34) = 5.02, p = .01, η_p^2 = .23. Post-hoc tests revealed that accuracy was significantly higher on grouped-feature trials relative to letter-match trials and color-match trials (ps < .001), and letter-match trials showed higher accuracy in location-shared versus location unshared (p = .02). For the RT data, I conducted a 2 (location) x 3 (feature type) repeated-measures ANOVA. This analysis showed significant main effects of feature type, F (2, 34) = 49.19, p < .001, η_p^2 = .74, and location, F (1, 17) = 9.09, p = .008, η_p^2 = .35, and a significant interaction between feature type and location, F (2, 34) = 9.62, p < .001, η_p^2 = .36. These results indicated faster RT for grouped trials relative to letter-match and color-match trials and faster RT for location-shared relative to location-unshared trials on grouped-feature and letter-match trials but not on color-match trials (Figure 5).

Table 1

Mean Accuracy and Response Time of Correct Response in Each Condition

| | Two-Feature | | | |
| | Grouped | | Separated | No-Feature |
	Shared	Unshared		
RT (ms)	494.5 ± 55.2	510.9 ± 55.1	504.1 ± 55.9	671.1 ± 109.0
Accuracy (%)	98.5 ± 1.7	98.1 ± 3.4	98.5 ± 2.6	92.0 ± 7.4

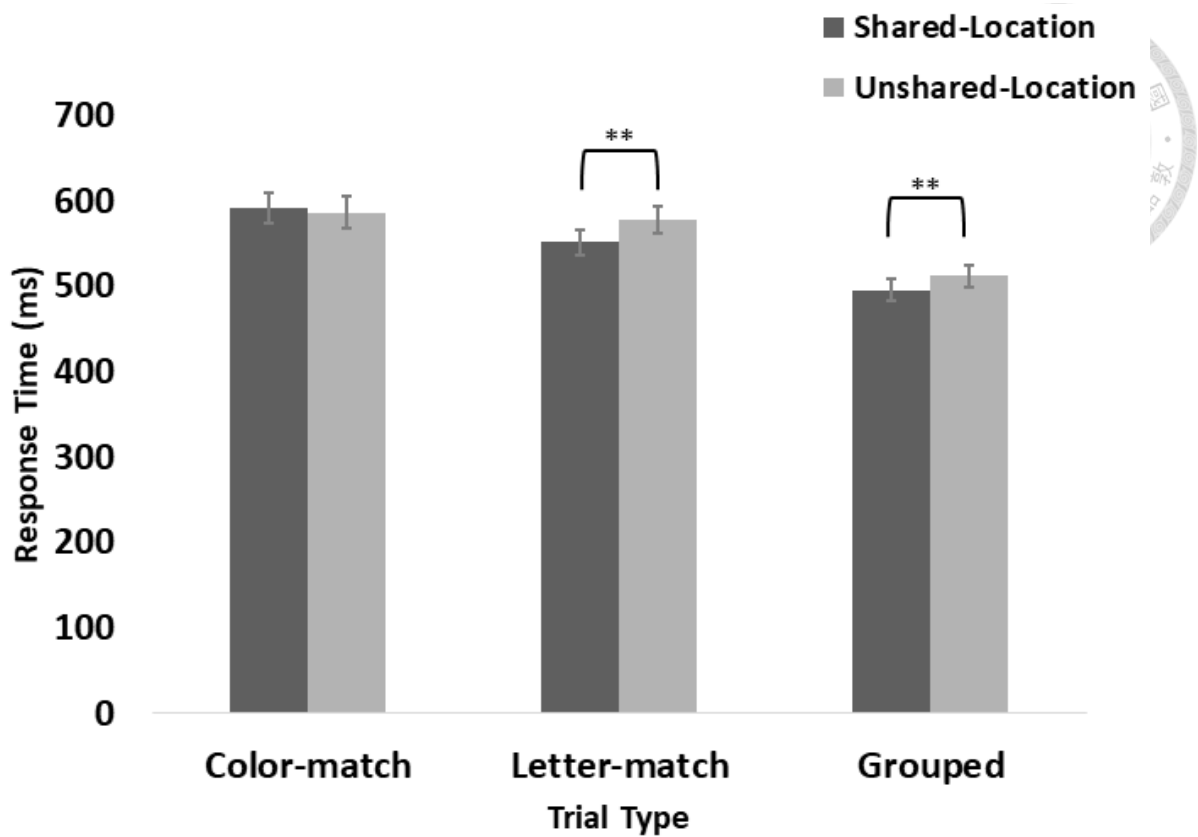| | One-Feature | | | |
| | Letter-Match | | Color-Match | |
	Shared	Unshared	Shared	Unshared
RT (ms)	550.5 ± 62.7	576.8 ± 64.0	590.6 ± 75.7	585.5 ± 78.9
Accuracy (%)	95.2 ± 3.6	92.6 ± 4.8	83.9 ± 10.6	85.6 ± 9.3

22

Figure 5. Mean response times across three types of trial with location-shared and location-unshared were compared. The results showed that the feature-bound representations were modulated by features' location on letter-match trials and grouped trials. Error bars indicate standard error of the mean (** $p < .01$).

RMI Results

The CDFs of the RT data are displayed in Figure 6. According to the previous study (Saiki, 2016), a cross between the curve of the CDF from the summation of two one-feature trials and the curve from the two-feature trials indicated feature coactivation. I thus firstly tested for feature coactivation effects on grouped and separated trials, respectively. On grouped trials, the violation of RMI was observed at the 5th to 25th percentiles [5th: t (17) = 3.11, p = .003; 10th: t (17) = 2.46, p = .012; 15th: t (17) = 2.99, p = .004; 20th: t (17) = 2.40, p = .015; 25th: t (17) = 2.28, p = .018 Figure 6a]. A significant violation was also found on separated trials at the 5th and 10th percentiles [5th: t (17) = 2.30, p = .017; 10th: t (17) = 1.81, p = .044, Figure 6b]. Importantly, I examine the modulatory effect of location on feature-bound representations. The RMI tests (summed feature trials versus grouped trials) were conducted for shared location and unshared location respectively. In the location-shared conditions, the RMI violation was observed at the 5th to 20th percentiles [5th: t (17) = 3.76, p < .001; 10th: t (17) = 3.86, p < .001; 15th: t (17) = 2.92, p = .005; 20th: t (17) = 2.47, p = .012, Figure 6c]. The RMI violation was also found in the location-unshared conditions at the 10th and 15th percentiles [10th: t (17) = 1.90, p = .037; 15th: t (17) = 2.09, p = .026, Figure 6d]. Overall, the RMI violation can be observed regardless of location sharing.
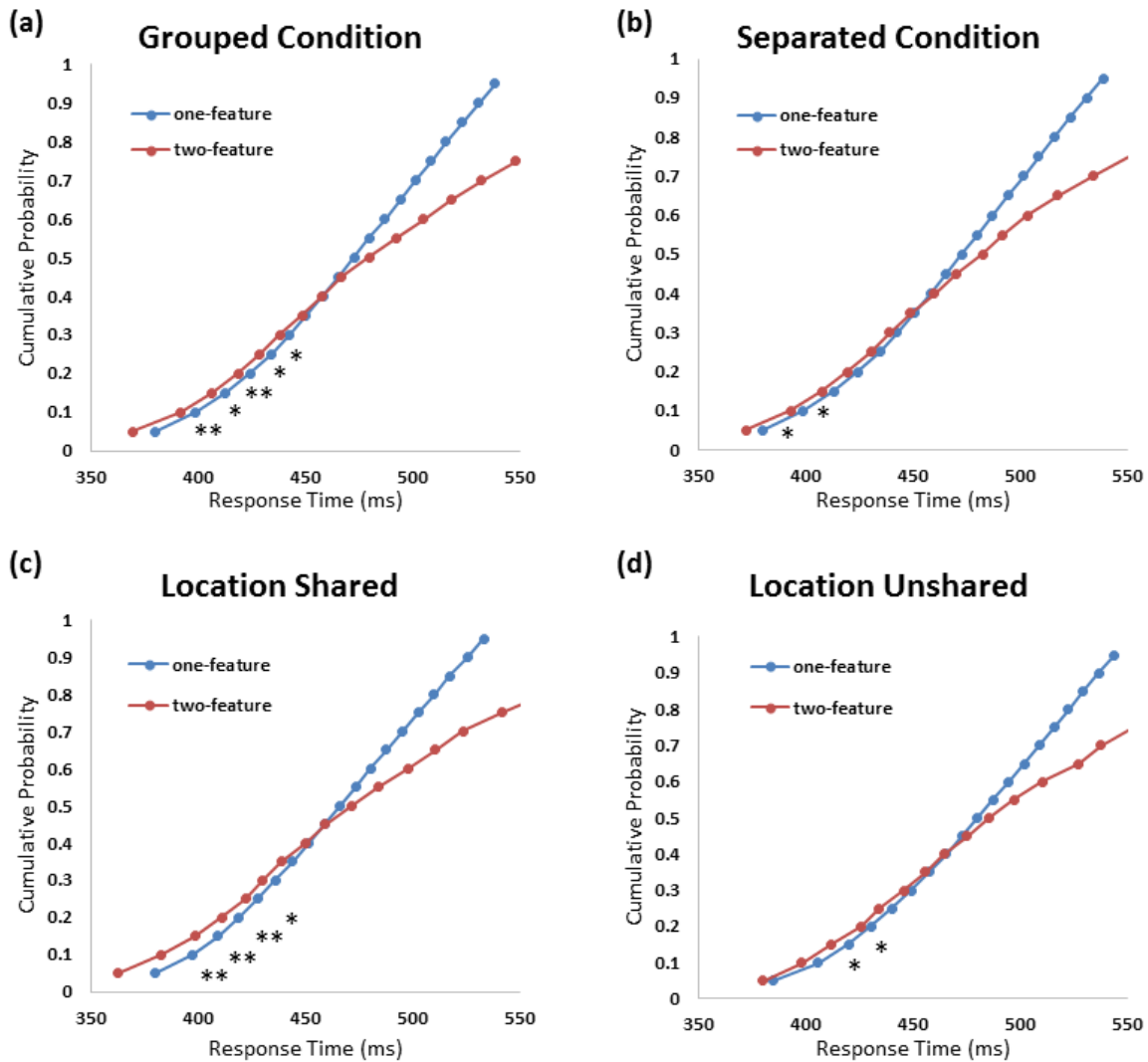
Figure 6. Cumulative density function (CDF) of RTs for the RMI test. Each graph shows the cumulative probability for RT for the two-feature condition and for the sum of the CDFs on letter- and color-match trials in the one-feature condition. (a) The CDFs of RTs in the grouped condition and one-feature condition. (b) The CDFs of RTs in the separated condition and one-feature condition. (c) The CDFs of RTs in the grouped-shared condition and one-feature-shared condition. (d) The CDFs of RTs in the grouped-unshared condition and one-feature-unshared condition. Asterisks indicate a significant difference between mean percentile RT (*$p < .05$, **$p < .01$, determined by one-tailed paired t tests).

MEG Results

Time-frequency results and neural origins of gamma oscillations. I firstly tested the modulation of location on gamma power lateralization (contralateral relative to ipsilateral site to the probe hemifield) at the sensor level when the participants compared the incoming probe item with the WM contents. Four contrasts were conducted: (1) grouped-shared-feature vs. one-shared-feature, (2) grouped-unshared-featured vs. one-unshared-feature, (3) grouped-shared-feature vs. separated-feature, and (4) grouped-unshared-feature vs. separated-feature. I observed significant effects of sensors in all contrasts. Significant effects of sensors were observed over the posterior parietal sensors from 580 to 612 ms for grouped-shared-feature vs. one-shared-feature trials (corrected $p = .013$), over the frontal and parietal sensors from 500 to 530 ms for grouped-unshared-feature vs. one-unshared-feature trials (corrected $p = .033$), over the frontal and parietal sensors from 500 to 600 ms for grouped-shared-feature vs. separated-feature trials (corrected $p = .03$), and over the frontal and parietal sensors from 520 to 550 ms for grouped-unshared-feature vs. separated-feature trials (corrected $p = .024$). The beamformer source analysis showed stronger neural responses for in gamma rhyme in the right parietal cortex by contrasting left hemifield with right hemifield for both shared location and unshared location trials. These results are illustrated in Figure 7.
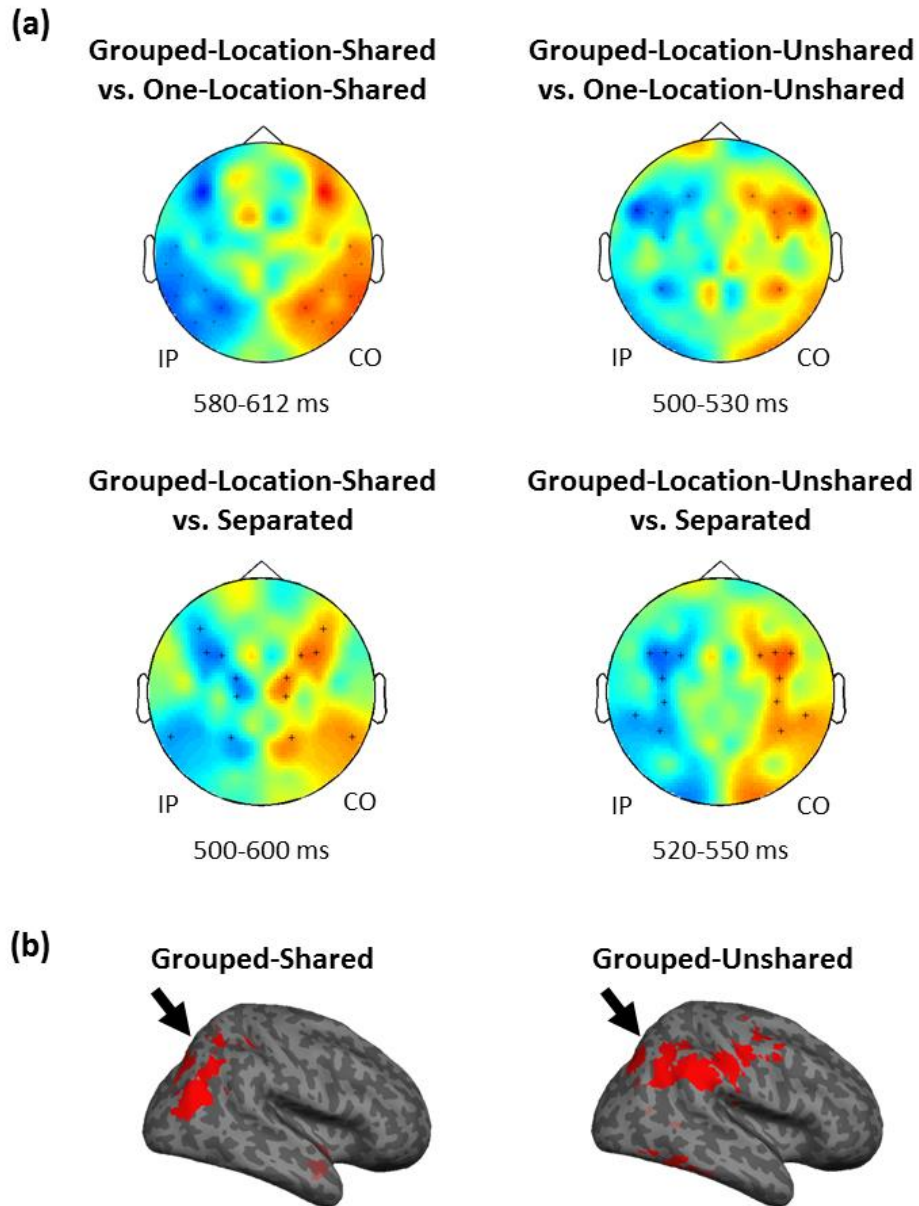
Figure 7. Sensor space and cortical source of gamma oscillation results. (a) Scalp topography of the difference in gamma lateralization between grouped-shared and one-shared trials. The gamma lateralization over frontal and parietal areas was observed when compared grouped-feature trials to one-feature trials in shared and unshared conditions respectively. (b) The gamma source results on grouped-shared, grouped-unshared, one-shared, and one-unshared trials respectively. The DICS beamformer analysis showed stronger gamma only in grouped-shared and grouped-unshared conditions.

27

Event-related fields and ROI source analyses. Finally, I tested the neural correlates of feature coactivation effect (Saiki, 2016) in the posterior brain regions and the difference in neural activity among three two-feature conditions (i.e. grouped-shared, grouped-unshared, and separated trials) during the WM-perceptual comparison. These results are illustrated in Figure 8. The mean ERFs were extracted from the posterior sensors (see Figure 8 for an example). A 2 (time window: 250-400 ms, 400-550 ms) x 3 (two-feature condition) repeated-measures ANOVA was then conducted. There was a significant main effect of two-feature condition, $F(2,34) = 11.61$, $p < .001$, and a significant interaction between time window and condition, $F(2,34) = 3.19$, $p = .05$. This interaction arose from greater activity on separated trials relative to both grouped-shared ($p = .002$) and grouped-unshared ($p < .001$) during the late time window (400-550 ms). However, no difference in activity was observed during the early time window. The source analysis using the LCMV beamformer showed greater neural responses in the right parietal cortex for the separated trials relative to grouped-shared and grouped-unshared trials respectively. The ROI-based analyses in the right parietal and visual ROIs confirmed these results (Figure 9).
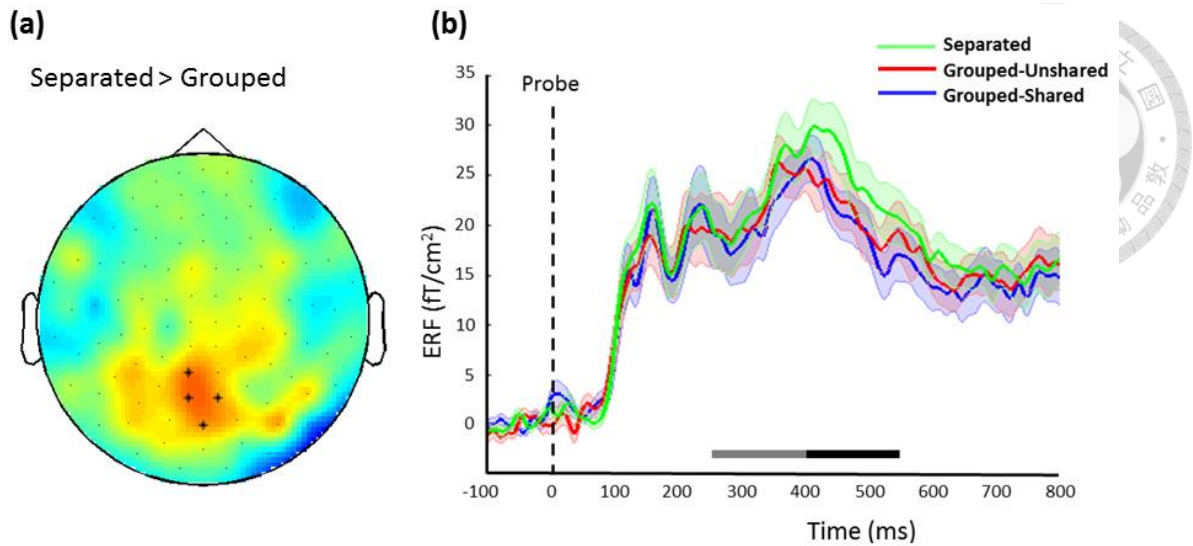
Figure 8. Sensor-space ERF results on grouped-shared, grouped-unshared, and separated

trials. The gray bar and black bar indicated the early and late time window in the analysis.

(a) Topography of the difference between separated and grouped trials from 428 to 460 ms.

(b) The power value of each condition was extracted from the sensor in the blue square.

The activity from 400 to 550 ms in separated condition was significantly higher than those

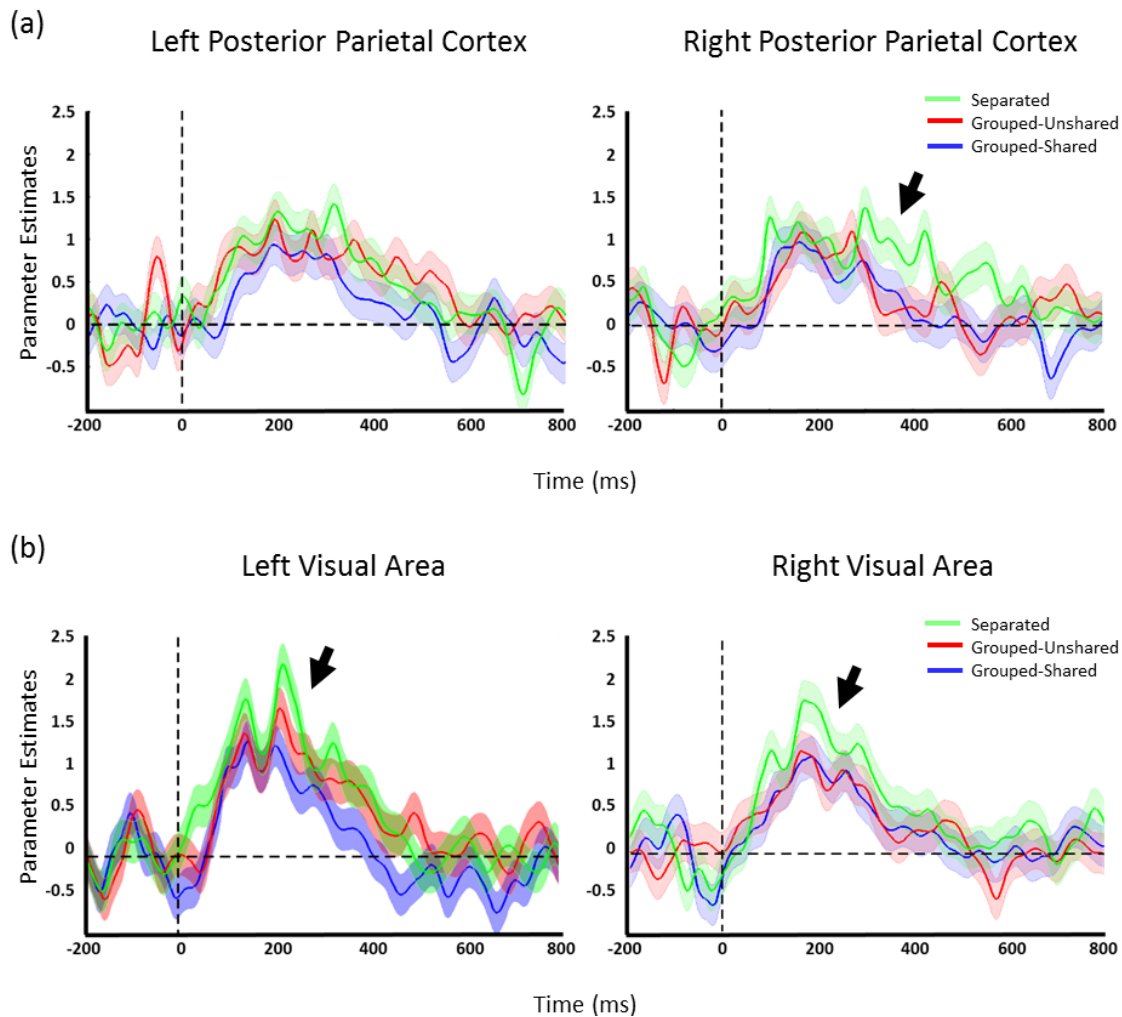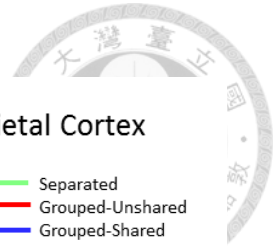in grouped-shared and grouped-unshared conditions.

Figure 9. Source and ROI-based results of ERF. The black arrows indicate the differential effect between separated and grouped conditions. (a) The source-level ERFs in left and right posterior parietal cortex show that there is greater activity on separated trials relative to grouped-shared and grouped-unshared trials. (b) The ERF in the bilateral visual ROI from the visual localizer task showed that there are also greater activities on separated trials relative to grouped-shared and grouped-unshared trials.

Discussion
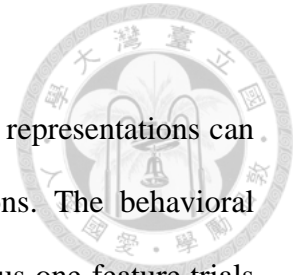
The purpose of this study was to investigate whether the feature-bound representations can be influenced by the location during the WM-perceptual comparisons. The behavioral results showed that participants responded faster on grouped trials versus one-feature trials for both shared-location and unshared-location. The RMI test also indicated that feature binding could occur independently of the location factor. Significant gamma activity was found in the parietal cortex for feature-bound representations regardless of the locations. Finally, the ERF data confirmed the effects of feature-bound in the posterior parietal and visual areas in both shared-location and unshared-location conditions. Together, these results provide further evidence in behavioural and neural correlates of WM-perceptual comparisons and suggest that feature-bound representations are not necessarily modulated by their locations.

In line with the previous findings, the behavioral data suggest that the integrated objects, instead of individual features, form the WM contents (Edin et al., 2009; Luck & Vogel, 1997; Luck & Vogel, 2013; Zhang & Luck, 2008). These studies also suggest that the feature binding can be implicit and automatic in WM. My results also replicate the behavioral findings from the recent study by Saiki (2016). I showed that feature binding can be observed in the two-feature condition when color and letter were grouped into a single object. Moreover, the violations of the RMI tests were found on both shared- and unshared-location trials. However, these results were inconsistent with the predictions by the object file theory (Kahneman et al., 1992; Noles, Scholl, & Mitroff, 2005). The object file account proposed that feature integration may occur when the probe was present at the

31

same location as the memory items. The RT RMI tests in the current study did not fully support the object file account (see Saiki, 2016 for a similar finding).
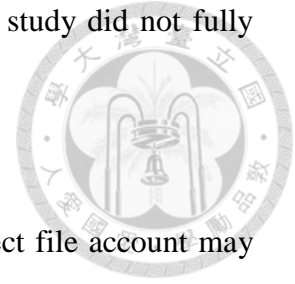
I speculate that the inconsistent results between my study and the object file account may arise from the feature types. In the current study, RMI tests showed that feature coactivation (letter and color) occurred in all two-feature conditions – not only grouped trials but also separated trials. However, Saiki (2016) reported the feature coactivation (shape and color) effect on grouped trials only. The effects of the one-feature and two-feature object were also different in location-sharing. For example, the location benefit in RT was observed on shape-match trials (Saiki, 2016) and on letter-match trials (the current study), not on color-match trials in both studies. Since previous studies have shown that WM performance may vary across stimulus types (Alvarez & Cavanagh, 2004; Treisman & Zhang, 2006), I suggest that feature types could influence the degree of features binding during WM-perceptual comparisons. Future work should systematically manipulate the feature types and test how they affect the features binding in WM.

The discrepancy from the current findings and Saiki's (2016) work may also result from the existence of non-target items. In the current study, I showed one probe item and a filler (i.e. a percentage sign) at the same time in boxes in each hemifield. This manipulation allows controlling the physical inputs from both visual hemifields across all feature types. However, the filler in the opposite hemifield may be likely to affect the allocation of attention on the target probe. Moreover, color and letter may reflect different levels of familiarity or superiority in real life (Mcclelland & Rumelhart, 1981). For example, if participants adopt a verbal strategy to perform the task, letter may cause stronger

32

interference with color in our case but shape may cause less interference with color. In sum, these factors may result in inconsistencies between the current results and others.

Importantly, I showed stronger lateralized gamma power with increased activity contralateral to the attended location and decreased activity contralateral to the unattended location for grouped object relative to single feature and for both shared and unshared locations. Similar modulations on lateralized gamma power were also found when I compared grouped-shared trials relative to separated trials and grouped-unshared trials relative to separated trials respectively. The results suggest that the gamma oscillations play an important role in feature integration in WM.

Studies in humans and monkeys have showed that increased activity in the gamma-band is related to attentional and mnemonic processes (Bauer, Oostenveld, Peeters, & Fries, 2006; Brovelli, Lachaux, Kahane, & Boussaoud, 2005; Buzsáki & Wang, 2012; Jensen, Kaiser, & Lachaux, 2007; Tallon-Baudry, Bertrand, Peronnet, & Pernier, 1998). For example, Fries, Reynolds, Rorie, and Desimone (2001) demonstrated that selective attention can influence the patterns of oscillatory synchrony between neural populations across different cortical areas with the enhancement of high-frequency oscillations (i.e. gamma) in occipital cortex. They showed that when attended items were represented by neurons that were able to communicate on such a fast temporal scale during gamma-frequency range, their impact was enhanced, leading to a more efficient selection of behaviorally relevant stimulus (see also Womelsdorf, Fries, Mitra, & Desimone, 2006). Moreover, other studies also found strong gamma activity during encoding and maintenance of WM (Mainy et al., 2007;

33

Sauseng & Klimesch, 2008; Tallon-Baudry et al., 1998). My results in lateralized gamma power are consistent with these findings.

The source results also suggest that gamma oscillation in parietal cortex may provide a putative mechanism for top-down control on feature binding. For example, an MEG study by Morgan et al. (2011) demonstrated greater gamma activity in the parietal cortex when colors and angles were integrated relative to single features during WM maintenance. A recent study using brain stimulation technique (e.g. transcranial alternative current stimulation) applied gamma frequency, theta frequency, and sham stimulations over the temporal and parietal cortex when participants were being performed a WM task with the manipulation of feature-only and color-shape binding (Tseng et al., 2016). They demonstrated that the anti-phase gamma stimulation had an influence on binding trials. Together, these results suggest that gamma oscillation is critical in the comparison process, particular in matching top-down (WM contents) and bottom-up (perceptual) information (Herrmann, Munk, & Engel, 2004).

While I did not observe any modulatory effect in early visual areas in the gamma band (Magazzini & Singh, 2018; Wilson, McDermott, Mills, Coolidge, & Heinrichs-Graham, 2018), the ERF results assured the feature binding effects in posterior parietal and early visual areas, indicating stronger activity for separated features relative to grouped-shared features and grouped-unshared features. To further examine the time course of ERF data, I divided the time-series into early and late time windows. This ERF analysis showed that the differential effects among two grouped feature conditions and separated feature conditions only occur in the late time window (400 ms – 550 ms). These results also support a recently
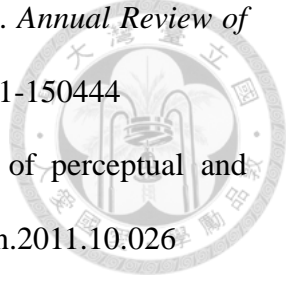
34

described load-dependent effect (e.g. N3rs) related to searching within WM (Kuo, Rao, Lepsien, & Nobre, 2009; Nobre, Griffin, & Rao, 2008). In their studies, the amplitude of the N3rs increase monotonically with the increasing load of retrospective search from within WM representations. The amplitude of the N3rs carried according to the degrees of feature coactivation, being smaller for grouped-shared features and grouped-unshared features compared to separated features. The N3rs therefore reflects time-consuming evaluation of the degrees of feature coactivation for putative probe items. Together with behavioral and gamma oscillation data, the ERF results also support the feature-bound representation independent to location congruency.
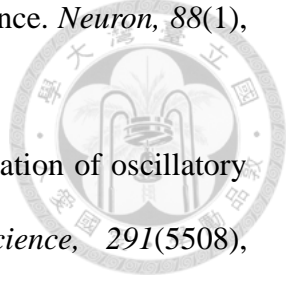
In conclusion, the current results from the behavioral and MEG data suggest that the location may have no or little influence on feature-bound representations during the comparisons of WM representation with perceptual information. These findings are compatible with previous findings that parietal cortex supports integration of visual features (Shadlen & Movshon, 1999; Shafritz et al., 2002). This study provides novel evidence in behavioral modeling and the oscillatory mechanisms which underlie the comparison of feature-bound and feature-unbound representations during the comparisons between WM and perception and the comparison process is associated with the gamma oscillation.

Reference

Allen, R. J., Baddeley, A. D., & Hitch, G. J. (2006). Is the binding of visual features in working memory resource-demanding? *Journal of Experimental Psychology: General, 135*(2), 298-313. doi:10.1037/0096-3445.135.2.298

Alvarez, G. A., & Cavanagh, P. (2004). The capacity of visual short-term memory is set both by visual information load and by number of objects. *Psychological Science, 15*(2), 106-111. doi:10.1111/j.0963-7214.2004.01502006.x

Awh, E., Vogel, E. K., & Oh, S. H. (2006). Interactions between attention and working memory. *Neuroscience, 139*(1), 201-208. doi:10.1016/j.neuroscience.2005.08.023

Baddeley, A. D. (1986). *Working memory*. New York: Oxford University Press.

Baddeley, A. D. (1992). Working memory. *Science, 255*(5044), 556-559. doi:10.1126/science.1736359

Baldauf, D., & Desimone, R. (2014). Neural mechanisms of object-based attention. *Science, 344*(6182), 424-427. doi:10.1126/science.1247003

Bauer, M., Oostenveld, R., Peeters, M., & Fries, P. (2006). Tactile spatial attention enhances gamma-band activity in somatosensory cortex and reduces low-frequency activity in parieto-occipital areas. *The Journal of Neuroscience, 26*(2), 490-501. doi:10.1523/jneurosci.5228-04.2006

Brainard, D. H. (1997). The Psychophysics Toolbox. *Spatial Vision, 10*(4), 433-436. doi:10.1163/156856897x00357

Brovelli, A., Lachaux, J.-P., Kahane, P., & Boussaoud, D. (2005). High gamma frequency oscillatory activity dissociates attention from intention in the human premotor cortex. *NeuroImage, 28*(1), 154-164. doi:10.1016/j.neuroimage.2005.05.045

Buzsáki, G., & Wang, X.-J. (2012). Mechanisms of gamma oscillations. *Annual Review of Neuroscience, 35*(1), 203-225. doi:10.1146/annurev-neuro-062111-150444

Chun, M. M., & Johnson, M. K. (2011). Memory: enduring traces of perceptual and reflective attention. *Neuron, 72*(4), 520-535. doi:10.1016/j.neuron.2011.10.026

Cowan, N. (1999). An embedded-process model of working memory. In A. Miyake & P. Shah (Eds.), *Models of working memory: mechanisms of active maintenance and executive control* (pp. 62-101). Cambridge, UK: Cambridge University Press.

Cowan, N. (2001). The magical number 4 in short-term memory: A reconsideration of mental storage capacity. *Behavioral and Brain Sciences, 24*(1), 87-114. doi:10.1017/S0140525X01003922

Duncan, J. (2001). An adaptive coding model of neural function in prefrontal cortex. *Nature Reviews Neuroscience, 2*(11), 820-829. doi:10.1038/35097575

Duncan, J. (2013). The structure of cognition: attentional episodes in mind and brain. *Neuron, 80*(1), 35-50. doi:10.1016/j.neuron.2013.09.015

Edin, F., Klingberg, T., Johansson, P., McNab, F., Tegnér, J., & Compte, A. (2009). Mechanism for top-down control of working memory capacity. *Proceedings of the National Academy of Sciences of the United States of America, 106*(16), 6802-6807. doi:10.1073/pnas.0901894106

Feintuch, U., & Cohen, A. (2002). Visual attention and coactivation of response decisions for features from different dimensions. *Psychological Science, 13*(4), 361-369. doi:10.1111/j.0956-7976.2002.00465.x

Fitousi, D. (2018). Feature binding in visual short term memory: A General Recognition Theory analysis. *Psychonomic Bulletin & Review, 25*(3), 1104-1113. doi:10.3758/s13423-017-1303-y

Fries, P. (2015). Rhythms for cognition: communication through coherence. *Neuron, 88*(1), 220-235. doi:10.1016/j.neuron.2015.09.034

Fries, P., Reynolds, J. H., Rorie, A. E., & Desimone, R. (2001). Modulation of oscillatory neuronal synchronization by selective visual attention. *Science, 291*(5508), 1560-1563. doi:10.1126/science.291.5508.1560

Fukuda, K., & Vogel, E. K. (2009). Human variation in overriding attentional capture. *The Journal of Neuroscience, 29*(27), 8726-8733. doi:10.1523/jneurosci.2145-09.2009

Gazzaley, A., & Nobre, A. C. (2012). Top-down modulation: bridging selective attention and working memory. *Trends in Cognitive Sciences, 16*(2), 129-135. doi:10.1016/j.tics.2011.11.014

Gross, J., Kujala, J., Hamalainen, M., Timmermann, L., Schnitzler, A., & Salmelin, R. (2001). Dynamic imaging of coherent sources: Studying neural interactions in the human brain. *Proceedings of the National Academy of Sciences of the United States of America, 98*(2), 694-699. doi:10.1073/pnas.98.2.694

Herrmann, C. S., Munk, M. H. J., & Engel, A. K. (2004). Cognitive functions of gamma-band activity: memory match and utilization. *Trends in Cognitive Sciences, 8*(8), 347-355. doi:10.1016/j.tics.2004.06.006

Hollingworth, A., & Rasmussen, I. P. (2010). Binding objects to locations: the relationship between object files and visual working memory. *Journal of Experimental Psychology: Human Perception and Performance, 36*(3), 543-564. doi:10.1037/a0017836

Honkanen, R., Rouhinen, S., Wang, S. H., Palva, J. M., & Palva, S. (2015). Gamma oscillations underlie the maintenance of feature-specific information and the contents of visual working memory. *Cerebral Cortex, 25*(10), 3788-3801.

doi:10.1093/cercor/bhu263

Jensen, O., Kaiser, J., & Lachaux, J.-P. (2007). Human gamma-frequency oscillations associated with attention and memory. *Trends in Neurosciences, 30*(7), 317-324. doi:10.1016/j.tins.2007.05.001

Jonides, J., Lewis, R. L., Nee, D. E., Lustig, C. A., Berman, M. G., & Moore, K. S. (2008). The mind and brain of short-term memory. *Annual Review of Psychology, 59*, 193-224. doi:10.1146/annurev.psych.59.103006.093615

Kahneman, D., Treisman, A., & Gibbs, B. J. (1992). The reviewing of object files: Object-specific integration of information. *Cognitive Psychology, 24*(2), 175-219. doi:10.1016/0010-0285(92)90007-O

Klimesch, W., Freunberger, R., & Sauseng, P. (2010). Oscillatory mechanisms of process binding in memory. *Neuroscience and Biobehavioral Reviews, 34*(7), 1002-1014. doi:10.1016/j.neubiorev.2009.10.004

Kondo, A., & Saiki, J. (2012) Feature-specific encoding flexibility in visual working memory. *PLoS One, 7*(12): e50962. doi:10.1371/journal.pone.0050962

Kuo, B. C., Rao, A., Lepsien, J., & Nobre, A. C. (2009). Searching for targets within the spatial layout of visual short-term memory. *The Journal of Neuroscience, 29*(25), 8032-8038. doi:10.1523/jneurosci.0952-09.2009
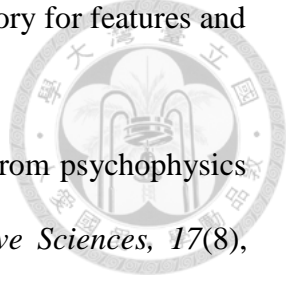
Landau, A. N., Schreyer, H. M., van Pelt, S., & Fries, P. (2015). Distributed attention is implemented through theta-rhythmic gamma modulation. *Current Biology, 25*(17), 2332-2337. doi:10.1016/j.cub.2015.07.048

Logie, R. H., Brockmole, J. R., & Jaswal, S. (2011). Feature binding in visual short-term memory is unaffected by task-irrelevant changes of location, shape, and color. *Memory & Cognition, 39*(1), 24-36. doi:10.3758/s13421-010-0001-z

Luck, S. J., & Vogel, E. K. (1997). The capacity of visual working memory for features and conjunctions. *Nature, 390*(6657), 279-281. doi:10.1038/36846

Luck, S. J., & Vogel, E. K. (2013). Visual working memory capacity: from psychophysics and neurobiology to individual differences. *Trends in Cognitive Sciences, 17*(8), 391-400. doi:10.1016/j.tics.2013.06.006

Luria, R., & Vogel, E. K. (2011). Shape and color conjunction stimuli are represented as bound objects in visual working memory. *Neuropsychologia, 49*(6), 1632-1639. doi:10.1016/j.neuropsychologia.2010.11.031

Magazzini, L., & Singh, K. D. (2018). Spatial attention modulates visual gamma oscillations across the human ventral stream. *NeuroImage, 166*, 219-229. doi:10.1016/j.neuroimage.2017.10.069

Mainy, N., Kahane, P., Minotti, L., Hoffmann, D., Bertrand, O., & Lachaux, J.-P. (2007). Neural correlates of consolidation in working memory. *Human Brain Mapping, 28*, 183-193. doi:10.1002/hbm.20264

Maris, E., & Oostenveld, R. (2007). Nonparametric statistical testing of EEG- and MEG-data. *Journal of Neuroscience Methods, 164*(1), 177-190. doi:10.1016/j.jneumeth.2007.03.024

Mcclelland, J. L., & Rumelhart, D. E. (1981). An interactive activation model of context effects in letter perception: I. An account of basic findings. *Psychological Review, 88*(5), 375-407. doi:10.1037/0033-295x.88.5.375

Miller, J. (1982). Divided attention: evidence for coactivation with redundant signals. *Cognitive Psychology, 14*(2), 247-279. doi:10.1016/0010-0285(82)90010-X

Minini, L., Parker, A. J., & Bridge, H. (2010). Neural modulation by binocular disparity greatest in human dorsal visual stream. *Journal of Neurophysiology, 104*(1),

169-178. doi:10.1152/jn.00790.2009

Mitra, P. P., & Pesaran, B. (1999). Analysis of dynamic brain imaging data. *Biophysical Journal, 76*(2), 691-708. doi:10.1016/S0006-3495(99)77236-X

Mordkoff, J. T., & Danek, R. H. (2011). Dividing attention between color and shape revisited: redundant targets coactivate only when parts of the same perceptual object. *Attention, Perception & Psychophysics, 73*(1), 103-112. doi:10.3758/s13414-010-0025-2

Mordkoff, J. T., & Yantis, S. (1991). An interactive race model of divided attention. *Journal of Experimental Psychology: Human Perception and Performance, 17*(2), 520-538. doi:10.1037/0096-1523.17.2.520

Morgan, H. M., Muthukumaraswamy, S. D., Hibbs, C. S., Shapiro, K. L., Bracewell, R. M., Singh, K. D., & Linden, D. E. J. (2011). Feature integration in visual working memory: parietal gamma activity is related to cognitive coordination. *Journal of Neurophysiology, 106*(6), 3185-3194. doi:10.1152/jn.00246.2011

Myers, N. E., Stokes, M. G., & Nobre, A. C. (2017). Prioritizing information during working memory: Beyond sustained internal attention. *Trends in Cognitive Sciences*, *21*(6), 449-461. doi:10.1016/j.tics.2017.03.010

Nobre, A. C., Griffin, I. C., & Rao, A. (2008). Spatial attention can bias search in visual short-term memory. *Frontiers in Human Neuroscience, 1*, 4. doi:10.3389/neuro.09.004.2007

Noles, N. S., Scholl, B. J., & Mitroff, S. R. (2005). The persistence of object file representations. *Perception and Psychophysics, 67*(2), 324-334. doi:10.3758/BF03206495

Nolte, G. (2003). The magnetic lead field theorem in the quasi-static approximation and its
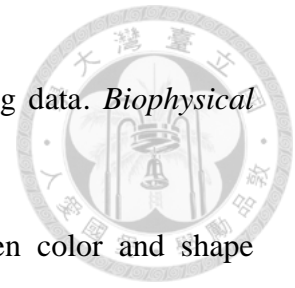
use for magnetoencephalography forward calculation in realistic volume conductors. *Physics in Medicine and Biology, 48*(22), 3637-3652. doi:10.1088/0031-9155/48/22/002
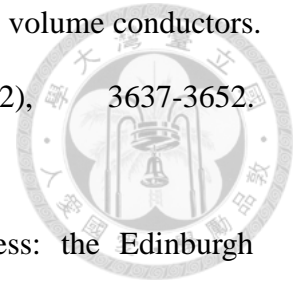
Oldfield, R. C. (1971). The assessment and analysis of handedness: the Edinburgh inventory. *Neuropsychologia, 9*(1), 97-113. doi:10.1016/0028-3932(71)90067-4

Oostenveld, R., Fries, P., Maris, E., & Schoffelen, J.-M. (2011). FieldTrip: open source software for advanced analysis of MEG, EEG, and invasive electrophysiological data. *Computational Intelligence and Neuroscience, 2011*, 9. doi:10.1155/2011/156869

Poch, C., Campo, P., & Barnes, G. R. (2014). Modulation of alpha and gamma oscillations related to retrospectively orienting attention within working memory. *The European Journal of Neuroscience*, *40*(2), 2399-2405. doi:10.1111/ejn.12589

Raab, D. H. (1962). Statistical facilitation of simple reaction times. *Transactions of the New York Academy of Sciences, 24*(5), 574-590. doi:10.1111/j.2164-0947.1962.tb01433.x

Ray, S., & Maunsell, J. H. (2015). Do gamma oscillations play a role in cerebral cortex? *Trends in Cognitive Sciences, 19*(2), 78-85. doi:10.1016/j.tics.2014.12.002

Roux, F., & Uhlhaas, P. J. (2014). Working memory and neural oscillations: alpha-gamma versus theta-gamma codes for distinct WM information? *Trends in Cognitive Sciences, 18*(1), 16-25. doi:10.1016/j.tics.2013.10.010

Roux, F., Wibral, M., Mohr, H. M., Singer, W., & Uhlhaas, P. J. (2012). Gamma-band activity in human prefrontal cortex codes for the number of relevant items maintained in working memory. *The Journal of Neuroscience, 32*(36), 12411-12420. doi:10.1523/jneurosci.0421-12.2012

Saiki, J. (2016). Location-unbound color-shape binding representations in visual working

memory. *Psychological Science, 27*(2), 178-190. doi:10.1177/0956797615616797

Saiki, J., & Miyatsuji, H. (2007). Feature binding in visual working memory evaluated by type identification paradigm. *Cognition, 102*(1), 49-83. doi:10.1016/j.cognition.2005.12.005

Sala, J. B., & Courtney, S. M. (2007). Binding of what and where during working memory maintenance. *Cortex, 43*(1), 5-21. doi:10.1016/S0010-9452(08)70442-8

Sauseng, P., & Klimesch, W. (2008). What does phase information of oscillatory brain activity tell us about cognitive processes? *Neuroscience & Biobehavioral Reviews, 32*(5), 1001-1013. doi:10.1016/j.neubiorev.2008.03.014

Schneegans, S., & Bays, P. M. (2017). Neural architecture for feature binding in visual working memory. *The Journal of Neuroscience, 37*(14), 3913-3925. doi:10.1523/jneurosci.3493-16.2017

Shadlen, M. N., & Movshon, J. A. (1999). Synchrony unbound: a critical evaluation of the temporal binding hypothesis. *Neuron, 24*(1), 67-77, 111-125. doi:10.1016/S0896-6273(00)80822-3

Shafritz, K. M., Gore, J. C., & Marois, R. (2002). The role of the parietal cortex in visual feature binding. *Proceedings of the National Academy of Sciences of the United States of America, 99*(16), 10917-10922. doi:10.1073/pnas.152694799

Tallon-Baudry, C., Bertrand, O., Peronnet, F., & Pernier, J. (1998). Induced gamma-band activity during the delay of a visual short-term memory task in humans. *The Journal of Neuroscience, 18*(11), 4244-4254. doi: 10.1523/ jneurosci.18-11-04244.1998

Treisman, A. M., & Zhang, W. (2006). Location and binding in visual working memory. *Memory & Cognition, 34*(8), 1704-1719. doi:10.3758/BF03195932

Tseng, P., Chang, Y. T., Chang, C. F., Liang, W. K., & Juan, C. H. (2016). The critical role

of phase difference in gamma oscillation within the temporoparietal network for binding visual working memory. *Scientific Report, 6*, 32138. doi:10.1038/srep32138

Van Dam, W. O., & Hommel, B. (2010). How object-specific are object files? Evidence for integration by location. *Journal of Experimental Psychology: Human Perception and Performance, 36*(5), 1184-1192. doi:10.1037/a0019955

Van Veen, B. D., Van Drongelen, W., Yuchtman, M., & Suzuki, A. (1997). Localization of brain electrical activity via linearly constrained minimum variance spatial filtering. *IEEE Transactions on Biomedical Engineering, 44*(9), 867-880. doi:10.1109/10.623056

Vogel, E. K., & Machizawa, M. G. (2004). Neural activity predicts individual differences in visual working memory capacity. *Nature, 428*(6894), 748-751. doi:10.1038/nature02447

Vogel, E. K., McCollough, A. W., & Machizawa, M. G. (2005). Neural measures reveal individual differences in controlling access to working memory. *Nature, 438*(7067), 500-503. doi:10.1038/nature04171

Wang, B., Cao, X., Theeuwes, J., Olivers, C. N., & Wang, Z. (2016). Location-based effects underlie feature conjunction benefits in visual working memory. *Journal of Vision, 16*(11), 12. doi:10.1167/16.11.12

Wheeler, M. E., & Treisman, A. M. (2002). Binding in short-term visual memory. *Journal of Experimental Psychology: General, 131*(1), 48-64. doi:10.1037/0096-3445.131.1.48

Wilson, T. W., McDermott, T. J., Mills, M. S., Coolidge, N. M., & Heinrichs-Graham, E. (2018). tDCS modulates visual gamma oscillations and basal alpha activity in occipital cortices: Evidence from MEG. *Cerebral Cortex, 28*(5), 1597-1609.

doi:10.1093/cercor/bhx055

Womelsdorf, T., Fries, P., Mitra, P. P., & Desimone, R. (2006). Gamma-band synchronization in visual cortex predicts speed of change detection. *Nature, 439*(7077), 733-736. doi:10.1038/nature04258
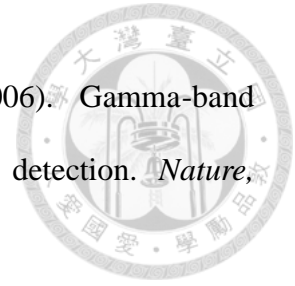
Yang, P., Fan, C., Wang, M., Fogelson, N., & Li, L. (2017). The effects of changes in object location on object identity detection: A simultaneous EEG-fMRI study. *NeuroImage, 157*, 351-363. doi:10.1016/j.neuroimage.2017.06.031

Zhang, W., & Luck, S. J. (2008). Discrete fixed-resolution representations in visual working memory. *Nature, 453*(7192), 233-235. doi:10.1038/nature06860